Bioactive Materials 21 (2023) 381–393

Contents lists available at ScienceDirect

Bioactive Materials

journal homepage: www.keaipublishing.com/en/journals/bioactive-materials

Passively-targeted mitochondrial tungsten-based nanodots for efficient acute kidney injury treatment

Qiong Huang [a,b], Yuqi Yang [a,b], Tianjiao Zhao [c,d], Qiaohui Chen [c,d], Min Liu [a,b], Shuting Ji [a,b], Yan Zhu [a,b], Yunrong Yang [a,b], Jinping Zhang [a,b], Haixin Zhao [c,d], Yayun Nan [e], Kelong Ai [c,d,*]

[a] Department of Pharmacy, Xiangya Hospital, Central South University, Changsha, 410008, China
[b] National Clinical Research Center for Geriatric Disorders, Xiangya Hospital, Central South University, Changsha, 410008, China
[c] Xiangya School of Pharmaceutical Sciences, Central South University, Changsha, 410078, China
[d] Hunan Provincial Key Laboratory of Cardiovascular Research, Xiangya School of Pharmaceutical Sciences, Central South University, Changsha, 410078, China
[e] Geriatric Medical Center, People's Hospital of Ningxia Hui Autonomous Region, Yinchuan, 750002, China

ARTICLE INFO

Keywords:
ROS-scavenging
Anti-inflammatory
Acute kidney injury
Passively-targeted mitochondrial
Tungsten-Based Nanodots

ABSTRACT

Acute kidney injury (AKI) can lead to loss of kidney function and a substantial increase in mortality. The burst of reactive oxygen species (ROS) plays a key role in the pathological progression of AKI. Mitochondrial-targeted antioxidant therapy is very promising because mitochondria are the main source of ROS in AKI. Antioxidant nanodrugs with actively targeted mitochondria have achieved encouraging success in many oxidative stress-induced diseases. However, most strategies to actively target mitochondria make the size of nanodrugs too large to pass through the glomerular system to reach the renal tubules, the main damage site of AKI. Here, an ultra-small Tungsten-based nanodots (TWNDs) with strong ROS scavenging can be very effective for treatment of AKI. TWNDs can reach the tubular site after crossing the glomerular barrier, and enter the mitochondria of the renal tubule without resorting to complex active targeting strategies. To our knowledge, this is the first time that ultra-small negatively charged nanodots can be used to passively target mitochondrial therapy for AKI. Through in-depth study of the therapeutic mechanism, such passive mitochondria-targeted TWNDs are highly effective in protecting mitochondria by reducing mitochondrial ROS and increasing mitophagy. In addition, TWNDs can also reduce the infiltration of inflammatory cells. This work provides a new way to passively target mitochondria for AKI, and give inspiration for the treatment of many major diseases closely related to mitochondria, such as myocardial infarction and cerebral infarction.

1. Introduction

Acute kidney injury (AKI), also known as acute renal failure, is a syndrome defined as a rapid increase in serum creatinine and nitrogen metabolism [1]. Kidney, as one of the most important metabolic and excretory organs, is easily injured by many factors, among which the most common factors are hemolytic and nephrotoxic drugs [2,3]. AKI is one of the main causes of death in hospitalized patients [4]. Approximately 421 million people are hospitalized each year, and the incidence of AKI in hospitalized patients is as high as 8%–18% (33.7–75.8 million people) [5]. AKI cause a significant increase in mortality by triggering remote multiple organ dysfunction through inter-organ crosstalk, such as liver dysfunction, cardiorenal syndrome, brain dysfunction, and systemic inflammation [6]. There is no definite therapy to treat AKI or prevent it from developing to chronic kidney disease (CKD) [7]. At present, the main clinical treatment are supportive treatment and renal replacement therapy (RRT) [3]. Specific measures are as follows: maintain effective renal blood flow perfusion through hemodynamic monitoring; maintain nutritional support (provide adequate protein intake) and control blood glucose level as much as possible; strictly monitor the use of nephrotoxic drugs, and discontinue nephrotoxic drugs to prevent aggravation of AKI; further RRT is required to reduce mortality from AKI once life-threatening water, electrolyte and acid-base balance is present [1]. However, the managements of AKI are often not always effective. For instance, over 50% of AKIs are mishandled in the UK [8]. Eventually, about 5% of AKI patients suffer from

Peer review under responsibility of KeAi Communications Co., Ltd.
* Corresponding author. Xiangya School of Pharmaceutical Sciences, Central South University, Changsha, 410078, China.
E-mail address: aikelong@csu.edu.cn (K. Ai).

https://doi.org/10.1016/j.bioactmat.2022.08.022
Received 19 May 2022; Received in revised form 5 August 2022; Accepted 20 August 2022

persistent renal insufficiency (needing long-term dialysis) or death [9]. Moreover, approximately 36.6% of hospitalized COVID-19 patients suffered from AKI [10]. Therefore, there is an urgent need for new strategies to prevent and treat AKI in the context of the ongoing global pandemic of COVID-19.

The main pathological manifestation of AKI is a serious renal tubule damage (especially the proximal convoluted tubules) due to the violent ROS burst at renal tubule site [11,12]. The main source of ROS is mitochondria because the electron transport chain of mitochondria is easily disturbed by various factors to generate ROS during AKI [12,13]. Excessive ROS damage biological membrane with reducing fluidity and enhancing permeability, and then leads to functional barriers such as cell membrane rupture, mitochondrial membrane swelling and dissolution. Excessive ROS also induce mitochondrial autophagy (mitophagy) but inhibit autolysosome degradation, lead to the impaired of dysfunctional mitochondria clearance, and ultimately cause a sharp decline in renal function [14]. Therefore, mitochondria-targeted antioxidant therapy is very promising in the treatment of AKI. Currently, many strong positive charge groups have been widely adopted as mitochondrial targeting groups, such as triphenyl phosphine [15], transition metal complexes [16], guanidines [17], mitochondrial targeting peptides (SS-31 and cell penetrating peptides) [18] because the inner mitochondrial membranes have a strong negative potential. These positively charged group modifications on nanodrugs must be further covered with negatively charged groups or electrically neutral groups for in vivo treatment, because the surface positively charged nanodrugs are easily cleared by the immune system and cannot reach the kidneys [19]. As a result, many mitochondria-targeted nanodrugs typically have sizes much larger than the glomerular filtration barrier and complex structure to achieve so-called sequential targeting to mitochondria in cells [20]. Therefore, not all mitochondria-targeted nanodrugs are suitable for AKI. Renal tubular damage is much earlier than the glomerulus in AKI [21]. Restricted by the glomerular filtration system, only nanodrugs with a size smaller than 10 nm can effectively pass through the glomeruli to reach the damaged renal tubules [22].

Polyoxometalate (POM), as an emerging anionic cluster material, has attracted widespread interests due to its unique physical and chemical properties [23]. Among them, Tungsten-based POM has been widely used in cancer treatment, antibacterial, anti-inflammatory, and other biomedicine fields because of its good biocompatibility and metabolism in vivo [24]. More importantly, well-designed Tungsten-based POM nanoparticles have a great potential to eliminate ROS because the W atom in W-POM has strong redox activity, and its redox potential is as low as 0.22 V and 0.47 V in aqueous solution [25]. Here, we develop an ultra-small Tungsten-based POM nanodots (TWNDs) with high antioxidant activity for the treatment of AKI. TWNDs contain a very high ratio of W^{+5}/W^{+6}, which can effectively eliminate $O_2^{\cdot-}$, $OH^{\cdot}$, H_2O_2, $ONOO^-$. It is worth mentioning that TWNDs have a super ability to remove $O_2^{\cdot-}$, and the superoxide dismutase (SOD) activity reaches 250U/mg. TWNDs effectively pass by the glomerulus to reach the renal tubules. More importantly, TWNDs can enter the mitochondria of renal tubular cells without any mitochondria-targeting groups because of the extremely high mitochondrial density of mitochondria in renal tubular cells. Similar to the heart, the kidney is one of the most energy-demanding organs in the body. The mitochondria number of proximal convoluted tubule epithelial cell is higher than that of other renal cell types because proximal convoluted tubules are mainly involved in the extremely energy-consuming reabsorption process [26]. To our knowledge, this is the first time that ultra-small nanodots with negatively charge can be used to passively target mitochondrial therapy for AKI. TWNDs nanodots effectively eliminate oxidative stress in the renal tubules thanks to their strong ability to eliminate ROS and passive targeting to the source of ROS (mitochondria), and only need about 1/32 dose of N-acetyl cysteine (NAC, traditional antioxidant drug) to effectively restore the function of hemolysis-induced AKI. The excellent therapeutic effect mainly originates from two mechanisms: 1) TWNDs efficiently protect the mitochondria by maintaining mitochondrial membrane potential, reducing the damage of mitochondrial respiratory chain, and restoring mitophagy; 2) TWNDs greatly reduce the infiltration of macrophages. In addition, TWNDs have good adaptability for the AKI treatment, and can also effectively restore renal function in the AKI induced by nephrotoxic drugs.

2. Results and discussion

2.1. Synthesis and characterization of TWNDs

TWNDs were prepared by reducing phosphotungstic acid with tannic acid under alkaline conditions (Fig. 1A). As shown as TEM, the diameter of TWND was about 2–4 nm (Fig. 1B). The flexible network-like structure of tannic acids effectively reduced phosphotungstic acid to form TWNDs with a high W^{5+} content (accounting for 53.4%) (Fig. 1C). Tannic acids also were successfully modified to the surface of TWNDs during the preparation process (Figs. S1–2). As a result, the surface of TWNDs was highly negatively charged (−35.4 mV) as measured by zeta potential (Fig. S3A). TWNDs were well-dispersed in an aqueous system, and the hydrodynamic diameter was only 8.2 nm (Fig. 1B insert), which was slightly larger than the measured value of TEM (Fig. S3B) because of the hydration of the surface ligands of TWNDs. Moreover, TWNDs had a higher X-ray computed tomography (CT) sensitivity than iohexol (the clinical CT contrast agent) because the X-ray attenuation coefficient of W element was far greater than I (4.438 vs 1.942 $cm^2\ g^{-1}$ at 100 keV) (Fig. 1D and E) [27]. The TWNDs exhibited visible light absorption spectra extended from the visible light region to the near infrared region (Fig. S4) due to the charge transfer between W^{5+} and W^{6+} through the W–O bond bridge. The high content of W^{5+} endowed TWNDs a very strong ability to eliminate a variety of ROS. TWNDs efficiently scavenged $O_2^{\cdot-}$, $OH^{\cdot}$, H_2O_2 and $ONOO^-$(Fig. 1F–I). Moreover, the scavenging of $O_2^{\cdot-}$ was particularly efficient, and the scavenging activity of TWNDs reached 250U/mg, which was about 18% of superoxide dismutase from bovine erythrocytes. The scavenging of various ROS was mainly achieved by W^{5+} of TWNDs, which accepted the electrons of ROS and transformed into W^{6+}(Fig. 1J, Fig. S5).

2.2. Distribution of TWNDs in vivo

Whether TWNDs passed through the glomerular filtration system was the key to the treatment of AKI [28] (Fig. 2A). We adopted CT imaging to track the distribution of TWNDs in vivo thanks to the high sensitivity of CT imaging of TWNDs. TWNDs efficiently flowed through the glomerular filtration system of the kidney to reach the bladder thanks to good hydrophilicity and small size of TWNDs in healthy (Fig. S6) and hemolysis-induced AKI mice (Fig. 2B and C). We also prepared water-soluble gold nanoparticles (Au NPs) with a diameter of 20–30 nm as a control (Fig. S7 A-B) [29]. In AKI or healthy mice, Au NPs were mostly distributed in the liver (Fig. S7 C-G) and can't pass through the glomerular barrier to the bladder (Fig. 2D) because the diameter of Au NPs was larger than the pore size of the glomerular filtration barrier. In addition, the bladder and kidney CT values of the AKI mice were also slightly higher than the healthy group (Fig. 2D), which may be attributed to the increased glomerular permeability caused by mild glomerular injury in AKI mice (Fig. 2E and F). We further adopted TEM to directly observe the distribution of TWNDs in the glomerular barrier of AKI mice. As shown as Fig. 2G, TWNDs were distributed in both glomerular capillaries and bowman's spaces, indicating that TWNDs effectively penetrated the glomerular filtration barrier. The content of element W in kidney, liver, blood, and feces at different time could be accurately reflected the distribution of TWND in vivo because TWND contained specific W element. As measured by inductively coupled plasma (ICP) of W, the TWNDs were distributed in the kidney to 2.93% ID/g at 2 h after injection, and only slightly decreased to 2.24% ID/g after 24 h (Fig. 2H). The blood half-life of TWNDs was approximately

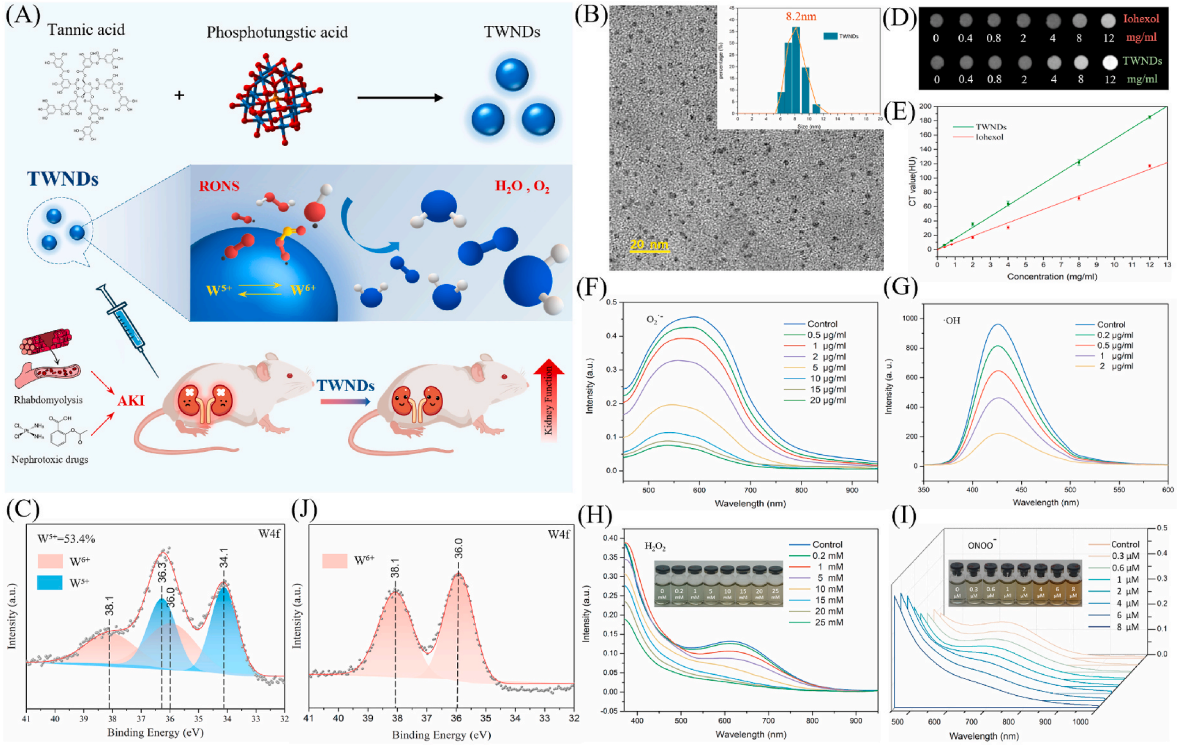

Fig. 1. Preparation and characterization of TWNDs. (A) Schematic illustration of preparation and treatment effect of TWNDs. (B) TEM image of TWNDs in water, scale bar: 20 nm. Insert: hydrodynamic diameter distribution of TWNDs. (C) and (J) X-ray photoelectron spectroscopy (XPS) spectrum of TWNDs before (C) and after (J) reaction with $O_2^{\cdot-}$. (D) CT images of TWNDs and Iohexol with different concentrations. (E) CT value (HU) of TWNDs/Iohexol as function of the concentration. (F–I) $O_2^{\cdot-}$ (F), H_2O_2 (G), $OH^{\cdot-}$ (H), and $ONOO^-$ (I) scavenging ability of TWNDs.

2–3 h in AKI or health mice by ICP (Fig. S8A). In addition, TWNDs persisted in the kidney of AKI mice for more than 3 days (Fig. S8B) despite TWNDs were excreted through the urinary system. Combined with the CT and tissue TEM results, these experiments fully demonstrate that TWNDs could be passively targeted to the site of AKI, which provided necessary conditions for TWNDs to scavenge ROS in AKI. For TWND, bioaccumulation was a must concern in AKI treatment. TWNDs were excreted not only through the urinary system, but also through the liver-feces route with the ICP test (Fig. S9A). After TWNDs treatment, the W content in the liver and kidney also gradually decreased with time (Fig. S8B, Fig. S9B), and almost disappeared after 30 days (Fig. 2H), indicating that TWNDs could be efficiently metabolized in vivo. W had similar chemical properties to Mo of the same group in the periodic table (Group 6 element). Mo was a common essential trace element and the active center of many key enzymes in mammals [30]. Therefore, W may be excreted through the Mo metabolic pathway in vivo.

2.3. Therapeutic effects of TWNDs

Hemolysis-induced AKI mouse model induced by intramuscular injection of glycerol [31] (Fig. 3A). To verify the therapeutic effect of TWNDs, NAC, a clinically approved antioxidant drug [32], was used as a control for AKI treatment. TWNDs effectively restored renal function with only about 1/32 of the dose of NAC (130 mg/kg), while the same dose of tannic acid had no therapeutic effect, and even aggravated AKI (Fig. 3B and C). In addition, the weight of the AKI mice also returned to normal after the TWNDs treatment (Fig. S10). Dihydroethidium (DHE) is a widely used redox-sensitive fluorescent probe and specific for ROS such as superoxide and hydrogen peroxide. The excellent therapeutic effect was mainly originated from the strong ability of TWNDs to scavenge ROS by assessing histologically (Fig. 3D). The effect of treatment was further explored through hematoxylin-eosin (HE) staining of kidney tissue. The glomerulus of AKI mice remained relatively intact, but the renal tubules showed severe damage: the renal tubules were obviously dilated and deformed, and there were many cell debris and casts in the lumen. In particular, the brush border of proximal convoluted tubule epithelial cells disappeared, epithelial cells were swollen, necrotic or exfoliated, and some nuclei are hyperchromatic and pyknotic. The damage to these renal tubules was effectively alleviated after TWNDs treatment (Fig. 3E). The tubular injury score further demonstrated that TWNDs were very effective in improving AKI (Fig. 3F). Moreover, the efficacy of TWNDs was verified by SOD activity, thiobarbituric acid reactive substances (TBARS), heme oxygenase-1(HO-1) and kidney injury molecule-1 (KIM-1) in kidney tissue. ROS further aggravated the damage of renal tubules by reducing the SOD activity, and elevated of renal injury markers (HO-1 and KIM-1) and TBARS by oxidizing lipids in renal tissue. TWNDs were very effective in reversing these indicators, which further confirmed the high therapeutic effect of TWNDs in AKI (Fig. 3G–J).

2.4. TWNDs as mitochondrial protectors

The recovery of renal function was heavily dependent on the reabsorption capacity of the renal tubules by protecting mitochondria [33]. The tubular region of healthy kidney tissue was densely populated by many mitochondria due to the high energy-consuming tubular demands [34]. In sham group, the mitochondria morphology was normal and the mitochondrial cristates were clearly discernible (Fig. 4A). In the renal tubular region of AKI, many mitochondria were ruptured, swollen and disintegration, the mitochondrial cristaes containing mitochondrial respiratory chain complexes were ruptured, and the mitochondrial matrix became loose (Fig. 4B). As mentioned earlier, TWNDs passed through the glomerulus to the tubular site in AKI (Fig. 4C). Through TEM of renal tissue, many TWNDs were confirmed to be distributed on mitochondria in renal tubules of AKI (Fig. 4D). It should be noted that TWNDs reached mitochondria without special mitochondrial targeting

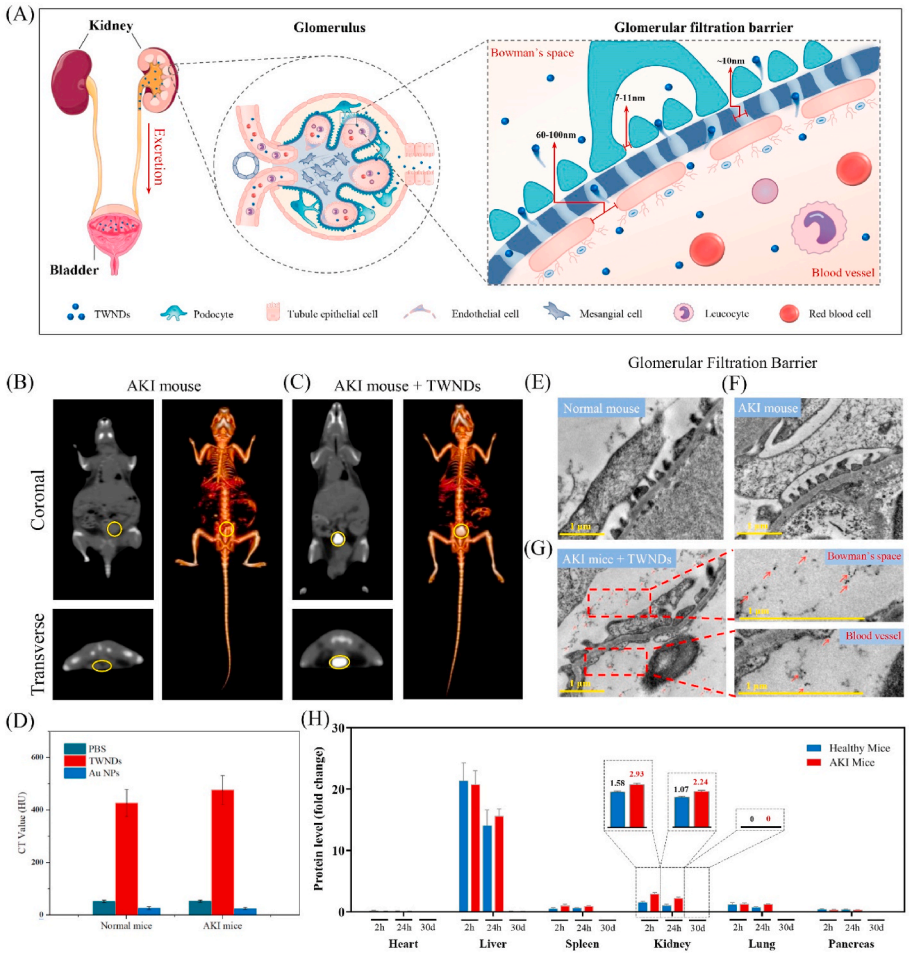

Fig. 2. Distribution of TWNDs in vivo. (A) Schematic illustration of TWNDs passively targeting to the kidney. (B) and (C) Serial CT coronal and transverse views and corresponding 3D renderings CT images of an AKI mouse after intravenous administration of PBS (B) and TWNDs (C). The yellow circle represents the location of bladders. (D) CT value (HU) of the bladder in different mice before and after injection of PBS, TWNDs and Au NPs. (E–G) TEM images of glomerular filtration barrier in normal mouse (E), AKI mouse (F) and AKI mouse after injection of TWNDs (G). Red dashed lines indicate the magnified area. The red arrows point to TWNDs. Scale bar: 1 μm. (H) Biodistribution of TWNDs in major organs at 2 h, 24 h and 30 days post injection.

strategies because of the extremely rich mitochondrial density of renal tubule cells. Moreover, the shape of mitochondria was effectively restored in AKI after TWNDs treatment (Fig. 4D). Cytochrome *c* (Cyt *c*) was an important component of the mitochondrial electron transport chain complex III and IV in the inner mitochondrial membrane [35]. Cyt *c* were released from the inner mitochondrial membrane to trigger cell apoptosis after high levels of ROS damaged inner mitochondrial membrane [36]. More importantly, mitochondria-generated ROS were released into the cytoplasm to trigger the increase of B-cell lymphoma 2-associated X protein (BAX) expression, and then BAX migrated to the mitochondrial membrane to damage the mitochondrial membrane, and finally formed a ROS-BAX-mitochondrial damage-Cyt c release-cell apoptosis cycle [37] (Fig. 4E). TWNDs were able to effectively inhibit the apoptotic cycle because TWNDs entered mitochondria through passive targeting strategies. Through immunohistochemistry staining of Cyt *c*, Cyt *c* were significantly reduced in the tubular region of AKI treated with TWNDs (Fig. 4L–M). Moreover, TWNDs significantly increased B-cell lymphoma 2 (BCL-2, an anti-apoptotic factor) expression, and decreased Cyt *c* release and BAX protein expression in AKI by kidney tissue western blot (WB) assay (Fig. 4F and G). The KIM-1 and NGAL expression levels were also greatly reduced in kidney tissue by TWNDs (Fig. 4F and G), further demonstrating that TWNDs effectively alleviated AKI. Cell apoptosis of the renal tubular was verified by terminal deoxynucleotidyl transferase dUTP nick end labeling (TUNEL) in AKI. As shown in Fig. 4J and K, TWNDs substantially reduced apoptosis in the renal tubular region in AKI. TWNDs also significantly reduced apoptotic bodies in the proximal convoluted tubule of AKI by kidney tissue TEM (Fig. S11). The scavenging of mitochondrial ROS by TWNDs was further verified at Human Kidney-2 cells (HK-2, a proximal convoluted tubule cell). H_2O_2 induced an increase in mitochondrial ROS levels in HK-2 cells, as confirmed by mitochondria-specific ROS probe (MitoSOX) (Fig. 4H–I, Fig. S12). The fluorescence intensity of MitoSOX was greatly reduced in the HK-2 treated with TWNDs, indicating that TWNDs passively targeted mitochondria and effectively reduced level of ROS at mitochondria. In addition, TWNDs also reduced H_2O_2-induced apoptosis in HK-2 cells (Fig. S13) by reducing mitochondrial damage (Fig. S14). In addition, ROS burst leaded to the weakening of renal tubular self-repair ability by inhibiting the proliferation of renal tubular cells. As shown as Fig. S15, TWNDs effectively restored the proliferation capacity of renal tubules through Ki67 staining of HK-2 cells.

In fact, mitochondria were always in homeostasis, and mitophagy effectively protected cells by eliminating damaged mitochondria [38]. As shown as TEM images (Fig. 5A–C), many autophagosomes covering damaged mitochondria were present in the TWNDs-treated or untreated AKI renal tubular region. The expression of mitophagy-related proteins PARKIN (an E3 ubiquitin ligase), PINK1 (PTEN-induced kinase 1), LC3BII/I (microtubule-associated protein 1 light chain 3 B, LC3B) of the AKI kidney was higher than that of sham mice because ROS induced mitophagy in the renal tubules of AKI (Fig. 5D and E). However, excessive ROS inhibited the degradation of autophagosomes in AKI (Fig. 5Di), resulting in the arrest of mitophagy at this last step. The p62/SQSTM1 encoded by the proto-oncogene C-myc was a protein synthesized in the cytoplasm and mediated the recruitment of ubiquitinated proteasomes to autophagosomes (Fig. 5Dii), which were critical for the subsequent degradation of damaged mitochondria in autolysosomes [39]. When the autophagy process was progressing smoothly, the content of p62/SQSTM1 decreased with the continuous degradation of p62/SQSTM1 in the autophagosomes. Once autophagy

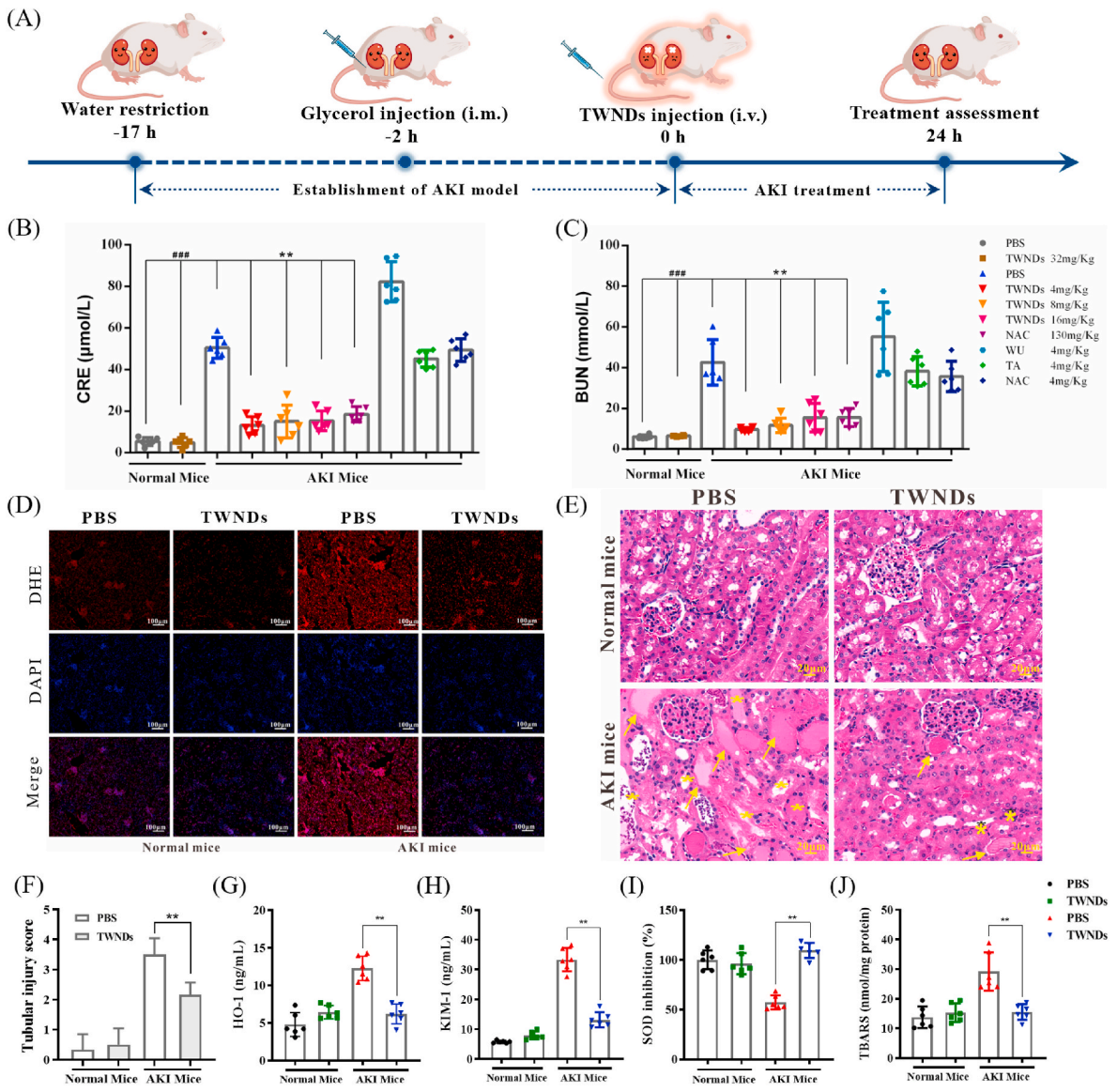

Fig. 3. Therapeutic effects of TWNDs. (A) Schematic illustration of the establishment and treatment schedule of AKI mice. Serum levels of CRE (B) and BUN(C) in normal mice or AKI mice at 24 h after different treatment. (D) DHE staining (red fluorescence), DAPI (blue fluorescence) staining, and their merge images of kidney tissues from each group. Scale bar: 100 μm. (E) HE staining of kidney tissues from each group. Yellow arrows indicate the damaged tubular epithelial cells and yellow stars indicate tubular casts. Scale bar: 20 μm. (F) Tubular injury score of each group in HE staining. (G–J) HO-1(G), KIM-1(H), SOD(I), and TBARS(J) levels measured in renal tissue homogenates from each group. Data represent means ± S.D. from six independent replicates. ($^{**}P < 0.01$ *vs* AKI + PBS group; $^{###}P < 0.001$ *vs* Normal + PBS or Normal + TWNDs group).

was blocked, the content of p62/SQSTM1 increased as p62/SQSTM1 accumulated in the cytoplasm. Therefore, p62/SQSTM1 was a sensitive biomarker to evaluate the inhibition of autophagic flux by ROS [40]. As shown in Fig. 5E, H, the p62/SQSTM1 level in the kidneys of AKI mice was much higher than that of normal mice, and TWNDs effectively reduced the level of p62 protein in AKI, suggesting that TWNDs greatly alleviated the ROS inhibition of autophagosomes to ultimately maintain mitochondrial homeostasis. As a result, PARKIN, PINK1 and LC3BII/I in the kidneys of TWNDs-treated AKI mice were slightly higher than those of healthy mice, but lower than those of AKI as mitophagy proceeds smoothly (Fig. 5E–G, I). The LC3B II ELISA result showed TWNDs significantly decreased the LC3B II expression (Fig. S16). The LC3B expression were increased in HK-2 cells treated with H_2O_2, and TWNDs decreased the LC3B expression in 1 h, 2 h, and 4 h (Fig. S17). These evidences further demonstrated that TWNDs effectively maintained mitochondrial homeostasis by increasing mitophagosome degradation in AKI. At last, mitochondrial function of AKI was effectively restored by TWNDs. TWNDs effectively maintained mitochondrial membrane potential in HK-2 cells with JC-1 dye as mitochondrial membrane potential probes (Fig. 5 J-K, Fig. S18). The recovery of mitochondrial function was closely related to mitochondrial membrane potential. As a result, ATP production rate also returned to near normal state after TWNDs treatment, which sufficiently proved that mitochondrial function was effectively restored (Fig. 5 L).

2.5. *Anti-inflammatory of TWNDs*

ROS led to generate many damage-associated molecular patterns (DAMPs) by inducing apoptosis of renal tubular epithelial cells. DAMPs (eg, ATP and calreticulin) generated "eat me" signals to recruit macrophages [41], followed by activation of pattern recognition receptors on macrophages to induce macrophage activation. Activated macrophages secreted many inflammatory factors such as interleukin 6 (IL-6), IL-1β and tumor necrosis factor α (TNF-α), and generated ROS through the

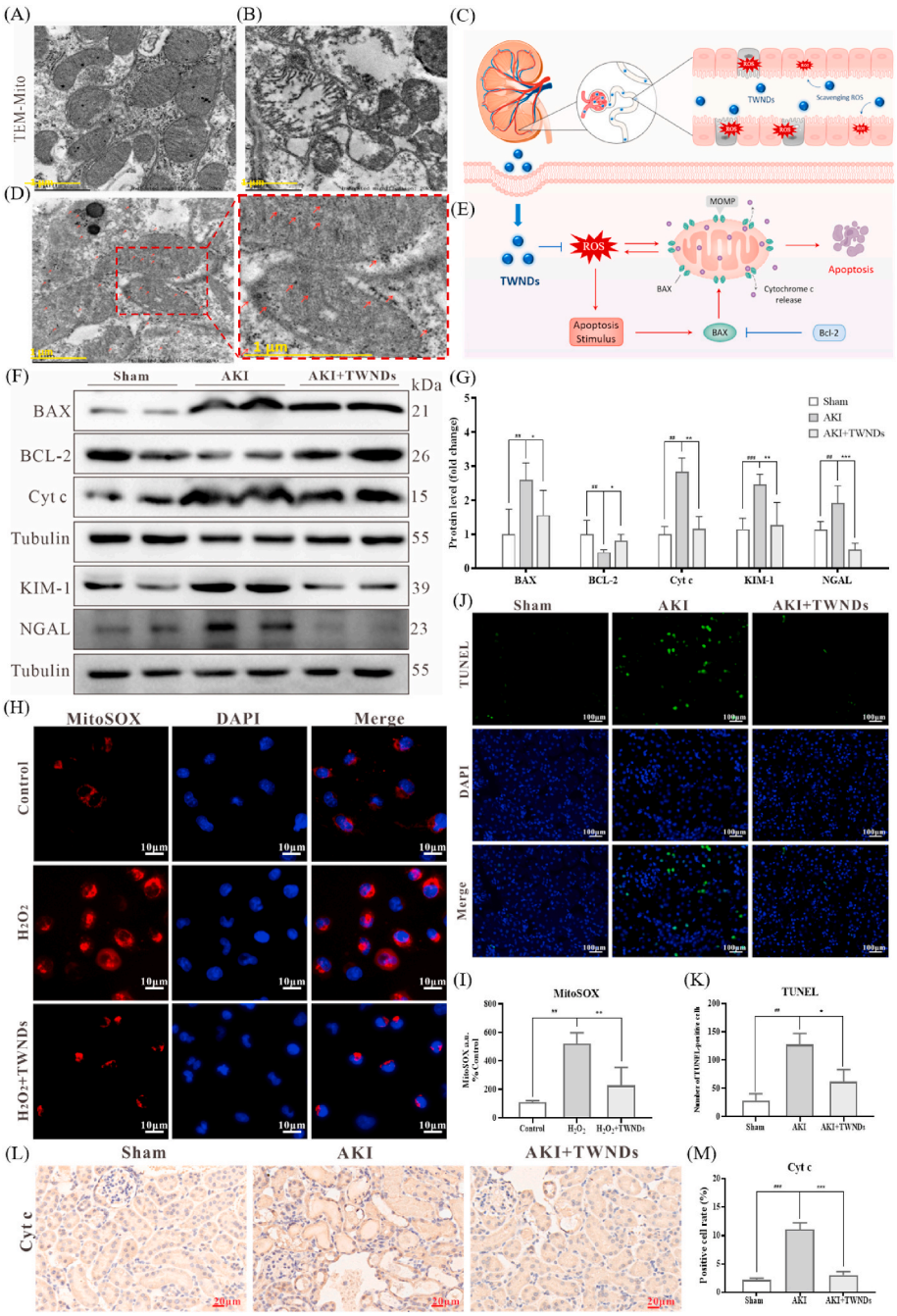

Fig. 4. TWNDs reduced mitochondrial-dependent apoptosis. (A–B) TEM image of mitochondria of tubular cells in normal mouse (A) and AKI mouse (B). Scale bar: 1 μm. (C) Schematic illustration of TWNDs passing through the glomerulus to the tubular site. (D) TEM image of mitochondria of tubule cells in AKI mouse after injection of TWNDs and the magnified image. Scale bar: 1 μm. (E) Schematic illustration of ROS induced mitochondrial-dependent cell apoptosis. (F) WB analysis of BAX, BCL-2, Cyt *c*, KIM-1 and NGAL proteins in renal tissue homogenate from each group. (G) Quantification of the protein immunoblots of BAX, BCL-2, Cyt *c*, KIM-1 and NGAL. (H) MitoSOX staining (red fluorescence), DAPI (blue fluorescence) staining, and their merge images of HK-2 cells from each group. Scale bar: 10 μm. (I) Quantification of MitoSOX-positive cells in (H). (J) TUNEL staining (green fluorescence), DAPI (blue fluorescence) staining, and their merge images of kidney tissues from each group. Scale bar: 100 μm. (K) Quantification of TUNEL-positive cells in (J). (L) Immunohistochemical staining of Cyt *c* from each group. Scale bar: 20 μm. (M) Quantification of Cyt-c-positive rate in (L). Data represent means ± S.D. from at least three independent replicates. (*$P < 0.05$, **$P < 0.01$, ***$P < 0.001$ *vs* AKI or H_2O_2 group; $^{\#\#}P < 0.01$, $^{\#\#\#}P < 0.001$*vs* sham or control group).

high expression of cyclooxygenase-2 (COX-2). Moreover, inflammatory factors such as TNF-α also induced apoptosis of tubular epithelial cells. Therefore, ROS formed a vicious circle with inflammation to aggravate AKI, and caused massive apoptosis of tubular epithelial cells in AKI [42]. TWNDs effectively broke the vicious cycle in the pathological process of AKI. Compared with the sham groups, the AKI groups had more infiltration of macrophages by F4/80 staining (Fig. 6A and B), and TWNDs greatly reduced the infiltration of macrophages in AKI (Fig. 6C and D) because TWNDs effectively reduced renal tubular apoptosis by eliminating ROS (Fig. 4F, J). The expression levels of inflammatory factors were further investigated in renal tissue. As show as Fig. S19, TWNDs significantly reduced the levels of inflammatory factors of AKI. Macrophage cells (RAW264.7) were used to further investigate the anti-inflammatory mechanism. RAW264.7 cells activation was induced by LPS in vitro and then ROS burst was generated by upregulating the expression of COX2. As shown as Fig. 6E–G, the COX-2 expression of activated RAW264.7 was greatly decreased by TWNDs. ROS and RNS were also greatly reduced and maintained near normal levels by TWNDs (Fig. 6H and I). Moreover, the secretion of IL-6, IL-1β, and TNF-α were detected in RAW264.7 cells, and TWNDs significantly reduced the increase in the secretion of inflammatory factors caused by LPS (Fig. 6J–L).

2.6. Adaptability and biocompatibility of TWNDs therapy

AKI, as a prevalent disease (especially for many elderly hospitalized patients), was very susceptible to many factors, like hemolytic and nephrotoxic drugs [2,43]. Excessive oxidative stress injury and inflammation were often core pathological progression factors in all types of AKI, although AKI induced by different factors often has some unique

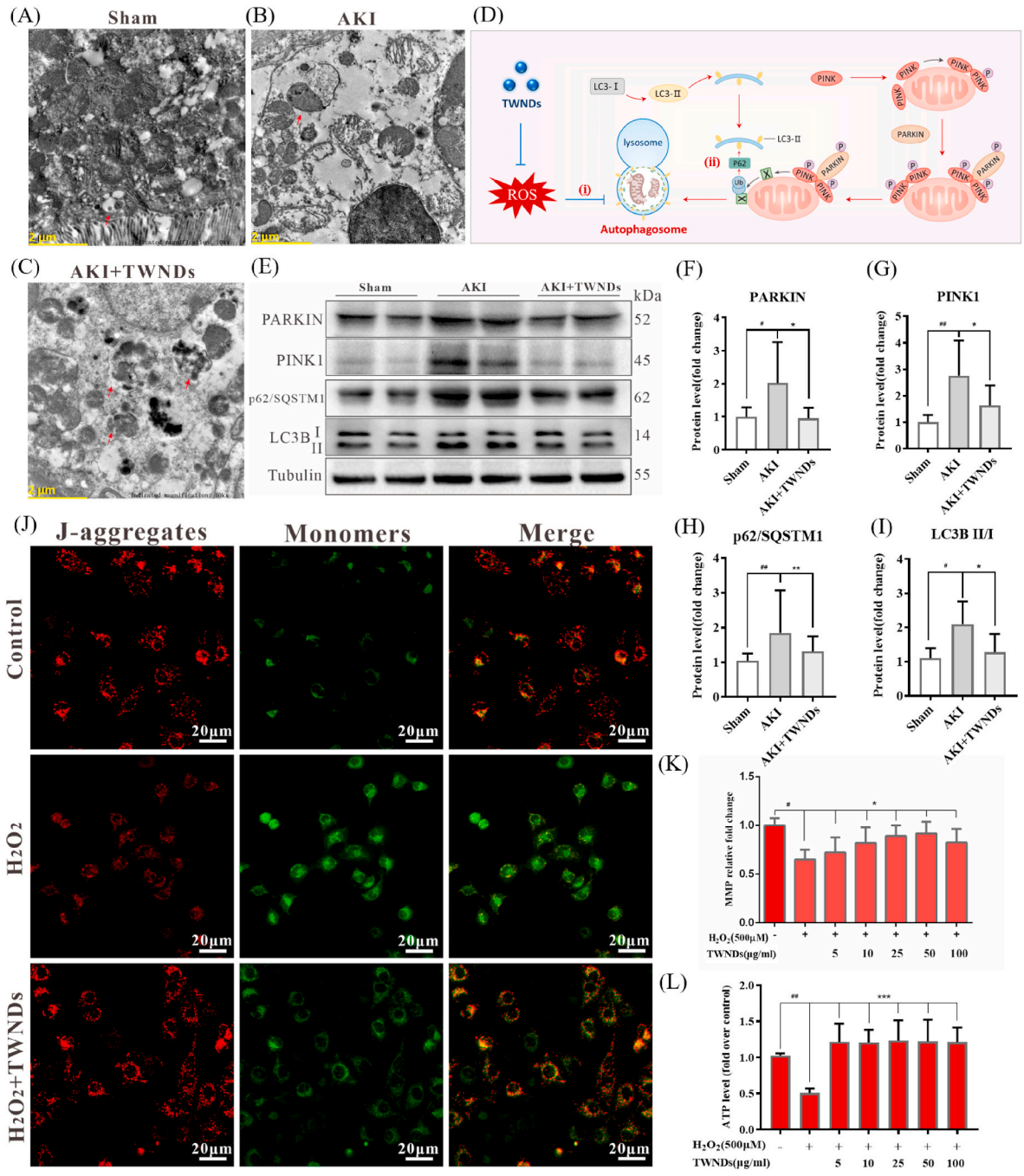

Fig. 5. TWNDs maintained the function of mitochondria and increased mitophagy. (A–C) TEM image of tubular cells in sham mouse (A), AKI mouse (B), AKI mouse after injection of TWNDs (C). Scale bar: 2 μm. (D) Schematic illustration of TWNDs restoring mitochondrial autophagy. (E) WB analysis of PARKIN, PINK1, p62/SQSTM1, and LC3BII/I proteins expression in renal tissue homogenate from each group. (F–I) Quantification of the protein immunoblots of PARKIN (F), PINK1 (G), p62/SQSTM1 (H), LC3BII/I (I). (J) Immunofluorescent staining of JC-1 in HK-2 cells from each group. Scale bar: 20 μm. (K) Quantification of mitochondrial membrane potential (MMP) of HK-2 cells under different treatments by Flow Cytometry. (L) ATP production rate of HK-2 cells under different treatments. Data represent means ± S.D. from at least three independent replicates. ($^{*}P < 0.05$, $^{**}P < 0.01$, $^{***}P < 0.001$ *vs* AKI or model groups; $^{\#}P < 0.05$, $^{\#\#}P < 0.01$ *vs* sham or control groups).

pathological features [44] (Fig. 7A). Through the above mechanistic analysis, TWNDs were very effective in protecting the kidney by reducing oxidative stress (through mitochondrial protection and increasing mitophagy pathways) and eliminating inflammation in rhabdomyolysis-induced AKI (Fig. 7B). Therefore, TWNDs should also have an excellent therapeutic effect in AKI induced by other factors. To verify the adaptability of the treatment of AKI, TWNDs were also adopted to treat cisplatin (CP)-induced AKI (CP-AKI). Many drugs were nephrotoxic, and drug-induced AKI was widespread in hospitalized patients. For example, CP, a first-line anticancer drug for many cancers, was one of the representative nephrotoxic drugs [45]. TWNDs were very effective for the treatment of CP-AKI and restores renal function (Fig. 7C) and histological morphology (Fig. 7D and E). The expression levels of KIM-1 and NGAL were significantly reduced after TWNDs treatment, further indicating that AKI restored renal function (Fig. 7F and G). TWNDs also reduced the apoptosis rate induced by CP in HK-2 cells (Fig. S20). The expression levels of BCL-2, BAX, and Cyt *c* (Fig. 7F and G) and the TUNEL staining (Figs. S21A–B) further illustrated that

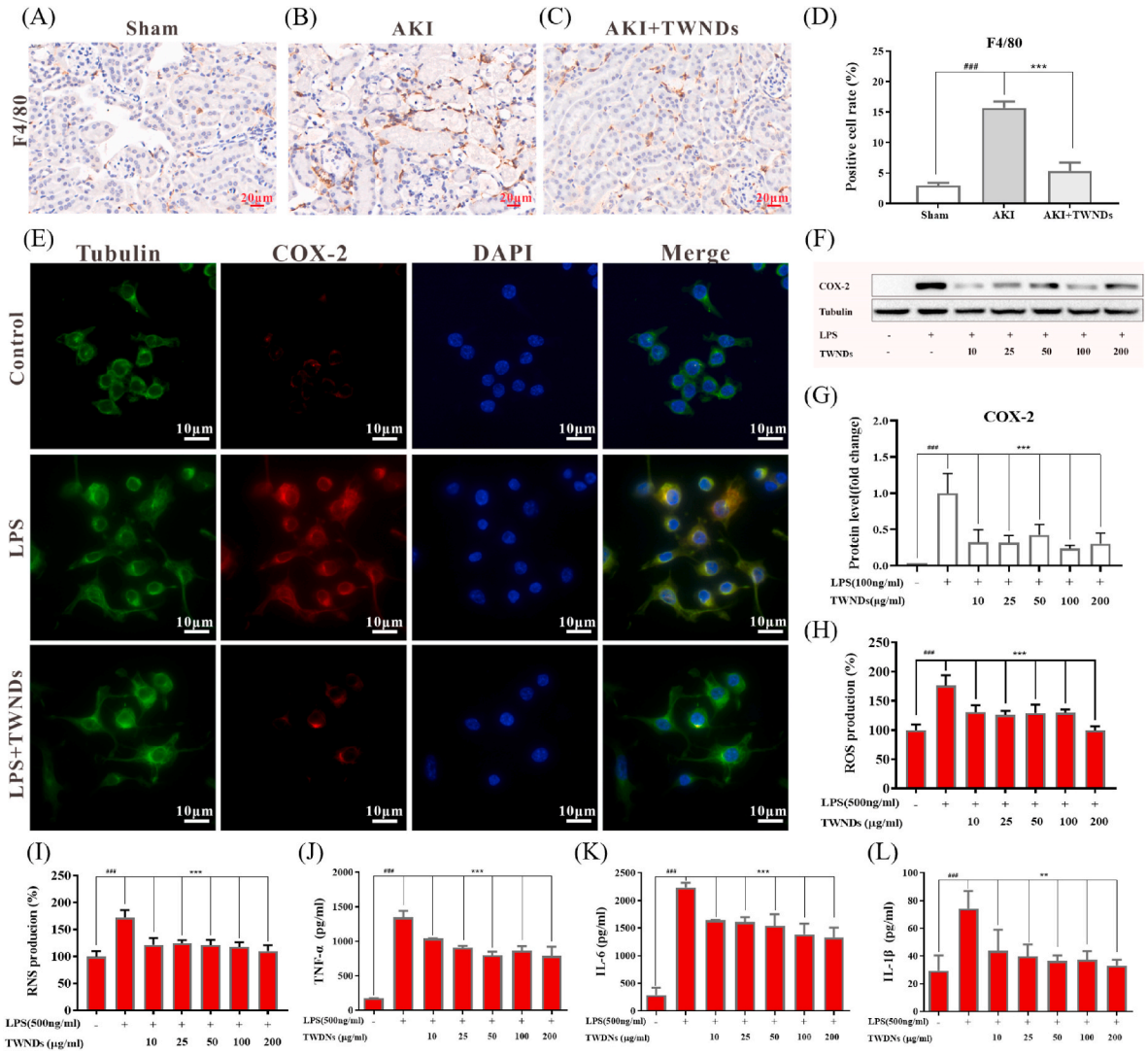

Fig. 6. Anti-inflammatory effect of TWNDs. (A–C) Immunohistochemical staining and quantification (D) of F4/80 of kidney sections from normal mice (A), AKI mice (B), AKI mice after injection of TWNDs (C). Scale bar: 20 μm. (E) Immunofluorescent staining and of Tubulin (green), COX-2 (red), DAPI (blue), and their merge images in RAW264.7 cells from each group. Scale bar: 10 μm. (F) WB analysis of COX-2 proteins in RAW264.7 cells from each group. (G) Quantification of the protein immunoblots of COX-2. (H) ROS and (I) RNS production rates of RAW264.7 cells from each group. (J–L) TNF-α (J), IL-6 (K) and IL-1β (L) production rates of RAW264.7 cells from each group. Data represent means ± S.D. from at least three independent replicates. (**$P < 0.01$, ***$P < 0.001$ *vs* LPS treated group; $^{###}P < 0.001$ *vs* control group).

TWNDs effectively reduced apoptosis in kidney tissue of CP-AKI. In addition, TWNDs effectively reduced the level of inflammation in CP-AKI (Figs. S21C–D).

Finally, the biocompatibility of nanomaterials was also investigated. TWNDs were almost non-toxic to HK-2 cells, and had a slight pro-proliferation effect at low concentration of TWNDs, while only up to 320 μg/ml had a slight anti-proliferative effect (Fig. S22). The effect of TWNDs on normal renal tubules was also further investigated in health mice by TUNEL and HE staining. As shown in Fig. S23, TWNDs didn't induce apoptosis of renal tubular cells in normal mice by TUNEL. Moreover, the renal tubules did not have lesions or necrosis, and the lumens were arranged in an orderly manner without swelling and cavities in the healthy mice treated with TWNDs (Figs. S24A–B), indicating that TWNDs did not affect the renal tubules cells of normal mice. In addition, TWNDs did not affect the function of normal kidneys (Fig. S24C) and livers (Fig. S24D). Moreover, TWNDs didn't have any damage to the heart, liver, spleen, lung, and kidney both in 1 day (Fig. S24B) and 1 month (Fig. S25) by HE staining. Moreover, TWNDs did not affect the inflammatory factors and blood cells counting (Fig. S24 E-G) in vivo.

3. Conclusion

TWNDs with ultra-small size not only have a very strong ability to eliminate a variety of ROS, but also has CT imaging capabilities. TWNDs have demonstrated a very impressive therapeutic effect of AKI, which can restore renal function at a very low dose. TWNDs can reach the renal tubular site through the glomerulus, and enter the mitochondria in the renal tubular epithelial cells by passive targeting because of the extremely high mitochondrial density of the renal tubular cells. The function of mitochondria is maintained by protecting mitochondria and increasing mitophagy efficiently with TWNDs. In addition, the apoptosis of renal tubular cells and the infiltration of macrophages can also be greatly reduced by TWNDs. In conclusion, TWNDs provide insights into the development of novel high-efficiency antioxidant nanodrugs with important theoretical and practical implications for AKI drug research.

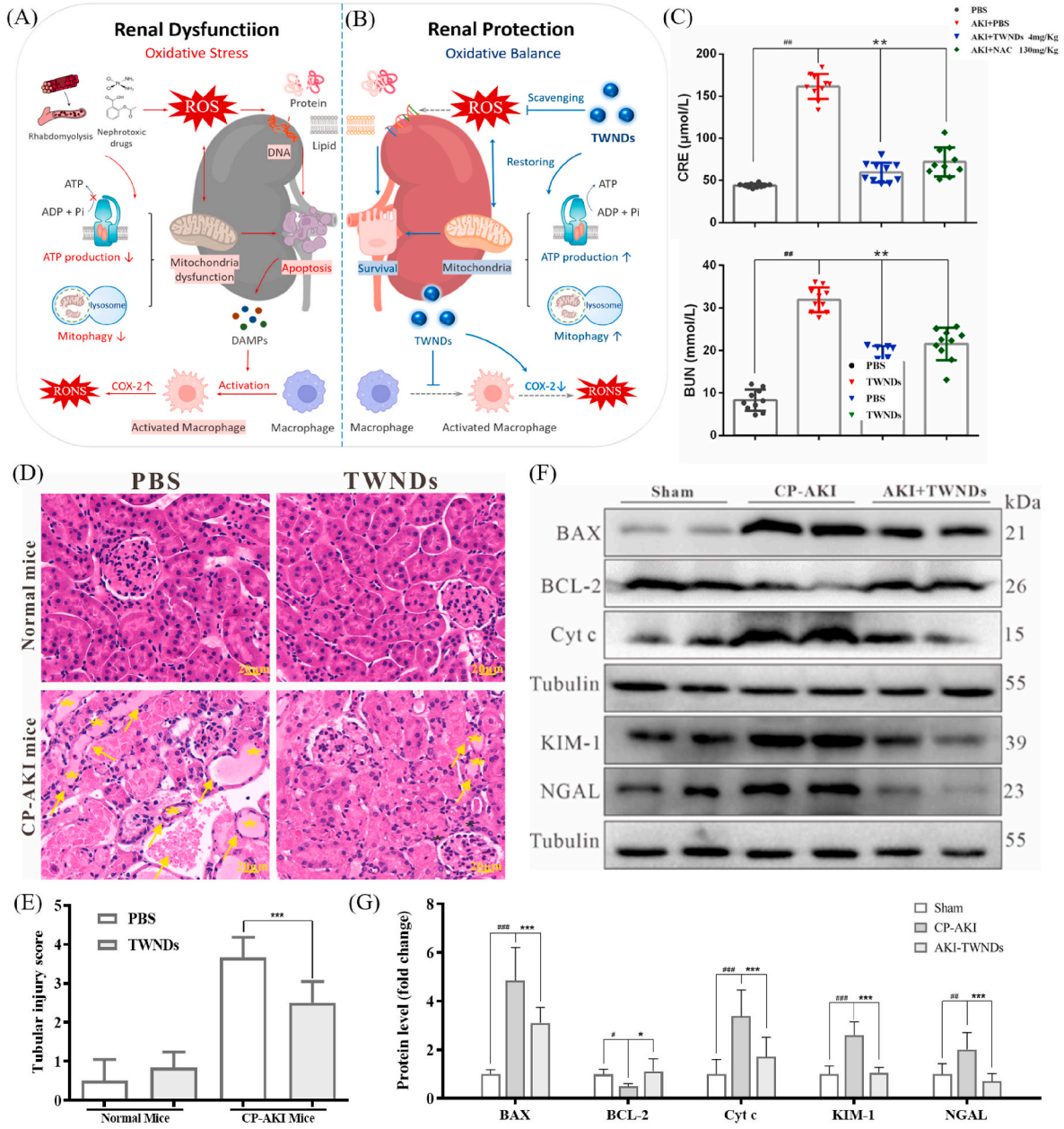

Fig. 7. Adaptability and biocompatibility of TWNDs therapy. (A–B) Schematic illustration of pathophysiological changes in kidneys of AKI before (A) and after (B) the application of TWNDs. (C) Serum levels of d CRE and BUN in normal mice or AKI mice at 24 h after different treatment. (D) HE staining of kidney tissues from each group. Yellow arrows indicate the damaged tubular epithelial cells and black stars indicate tubular casts. Scale bar: 20 μm. (E) Tubular injury score of each group in HE staining. (F) WB analysis of BAX, BCL-2, Cyt *c*, KIM-1 and NGAL proteins in renal tissue homogenate from each group. (G) Quantification of the protein immunoblots of BAX, BCL-2, Cyt *c*, KIM-1 and NGAL. Data represent means ± S.D. from six independent replicates. ($^{**}P < 0.01$, $^{***}P < 0.001$ vs AKI + PBS group, $^{\#\#}P < 0.01$, $^{\#\#\#}P < 0.001$ *vs* PBS group).

4. Materials and methods

4.1. Materials

CCK-8 and SOD assay kit were purchased from Dojindo Molecular Technologies (Kumamoto, Japan). Mouse KIM-1, HO-1, TNF-α and IL-6 ELISA kits and TBARS Colorimetric Assay kit were purchased from Elabscience Biotechnology (Houston, Texas, USA). A TUNEL assay kit (C10617), Caspase 3 polyclonal antibody (PA577887), Goat anti-Rabbit IgG (H + L) Highly Cross-Adsorbed secondary antibody Alexa Fluor 488 (A11034), Goat anti-Rabbit IgG (H + L) Cross-Adsorbed secondary antibody Alexa Fluor 555 (A21428), MitoSOX™ Red Mitochondrial Superoxide Indicator (M36008) and ProLong™ Glass Antifade Mountant with NucBlue™ Stain (P36983) were obtained from Thermo Fisher Scientific (Carlsbad,CA, USA). Enhanced mitochondrial membrane potential assay kit with JC-1(C2003S), Hoechst 33342 Staining Solution for Live Cells (C1028), and MDA were purchased from Beyotime Biotechnology (Shanghai, China). COX-2 antibody (CST,12282S) and F4/80 antibody (70076S) were purchased from Cell Signaling Technology (Danvers, MA, USA). BAX (ab32503), KIM-1 (ab78494) and Ki67 antibody (ab16667) were obtained from Abcam (Chicago, IL, USA). Bcl-2 antibody (BF9103), NGAL antibody (DF6816), tubulin beta antibody (AF7011), Goat Anti-Rabbit IgG (H+L) HRP (S0001) and Goat Anti-Mouse IgG (H + L) HRP (S0002) were obtained from Affinity Bioscience (Jiangsu, China). Cyt *c* antibody (d10933-1-AP) were purchased from Proteintech (Rosemont, IL, USA). CP was purchased from Sigma-

Aldrich (St. Louis, MO, USA).

4.2. Synthesis of TWNDs

TWNDs were synthesized by a redox reaction. Tannic acid (1.3 g) and phosphotungstic acid (0.72 g) were dissolved and mixed in ultra-pure water, and then anhydrous sodium carbonate (3.75 g) is added to create an alkaline environment. The reaction was allowed to proceed under magnetic stirring at room temperature (RT) for 12 h. Thereafter, phosphotungstic acid was reduced to a dark green solution, then the unreacted impurities were removed by dialysis, and TWNDs were obtained by freeze-drying.

4.3. Synthesis of 20–30 nm Au NPs

Au NPs were synthesized by a modification of our previous method. 200 ml of 0.25 mM chloroauric acid was stirred evenly and heated to boiling in a 500 ml round bottom flask. 20 ml of 50 mM sodium citrate solution was added to the chloroauric acid solution for 30 min to form gold nanoparticles, and then cooled to room temperature. 20 mg of bovine serum albumin was added to the gold nanoparticles solution to increase the stability of gold nanoparticles in vivo. Finally, gold nanoparticles were separated by centrifugation and washed twice with ultrapure water.

4.4. Characterization

TEM images were taken by using a TECNAI G2 high-resolution transmission electron microscope. XPS measurements were conducted with a VG ESCALAB MKII spectrometer. The XPSPEAK software (Version 4.1) was used to deconvolute the narrow-scan XPS spectra of the W 4f of the samples, using adventitious carbon to calibrate the C1s binding energy (284.5 eV). FTIR was recorded on a Bruker Vertex 70 spectrometer (2 cm^{-1}). UV/Vis spectra were collected using a VARIAN CARY 50 UV/Vis spectrophotometer. The fluorescence spectra were determined by using an F98 spectrofluorometer. The ICP measurements were conducted using the Thermo/Jarrell Ash Advantage Atomscan Inductively Coupled Argon Plasma Spectrometer.

4.5. In vitro and in vivo CT imaging

For in vitro CT imaging, TWNDs and clinical iodinated contrast agent (Iohexol) were dispersed in water with different concentrations in the range from 0 to 12 mg/ml. For in vivo CT imaging, the mice were first anesthetized by intraperitoneal injection of pentobarbital sodium solution (1 wt%), and then 0.1 mL of TWNDs (20 mg W mL^{-1}) dispersion in physiological saline and 0.1 mL of Iohexol (20 mg I mL^{-1}) were administrated intravenously into two mice, respectively. CT images were collected using a JL U.A NO.2 HOSP Philips iCT 256 slice scanner, imaging parameters were as follows: thickness, 0.9 mm; pitch, 0.99; 120 KVp, 300 mA; field of view, 350 mm; gantry rotation time, 0.5 s; table speed, 158.9 mm/s.

4.6. Superoxide anion scavenging with TWNDs

The NBT method was used to detect the $O_2^{-\cdot}$. The scavenging ability of TWNDs. In the presence of methionine, riboflavin undergoes photochemical reduction and further produce $O_2^{-\cdot}$. $O_2^{-\cdot}$ can reduce tetrazolium blue (NBT) to blue methyl hydrazine, which has maximum absorption at 560 nm. Briefly, methionine (20 μmol/L), riboflavin (0.01 mol/L), NBT (0.01 mol/L), TWNDs with different concentrations (0 μg/ml, 0.5 μg/ml, 1 μg/ml, 2 μg/ml, 5 μg/ml, 10 μg/ml, 15 μg/ml, 20 μg/ml), PBS (0.01 mol/L, pH7.4) and deionized water was added to the cuvettes and mixed. The cuvettes were then exposed to ultraviolet light for 5 min. The absorbance of blue methyl hydrazine was measured at 560 nm, and the $O_2^{-\cdot}$ scavenging ability was calculated by the intensity of TWNDs-inhibited NBT photochemical reduction.

4.7. Free radical scavenging with TWNDs

The $OH^{-\cdot}$ scavenging efficiency of TWNDs was determined by fluorescence spectrophotometry. The Fenton reaction between $FeSO_4$ and H_2O_2 catalyzes the formation of $OH^{-\cdot}$. The combination of non-fluorescent terephthalic acid and $OH^{-\cdot}$ can produce fluorescent 2-hydroxyl terephthalic acid. The addition of TWNDs can reduce the formation of the latter and reduce the fluorescence intensity. Terephthalic acid (0.1 mmol/L), ferrous sulfate (0.05 mmol/L), H_2O_2 (1 mmol/L) and PBS (0.01 mol/L, pH7.4) were prepared and mixed. Then TWNDs with different concentration (0 mM, 0.2 mM, 1 mM, 5 mM, 10 mM, 15 mM, 20 mM, 25 mM) were added to the reaction system. After standing for 6 min, the mixture was transferred to cuvettes and the corresponding fluorescence intensity was scanned under the excitation wavelength of 320 nm.

The H_2O_2 scavenging activity of TWNDs was determined by UV–Vis spectrophotometry. In brief, H_2O_2 (1 mmol/L) and TWNDs with different concentration (0 μg/ml, 0.2 μg/ml, 0.5 μg/ml, 1 μg/ml, 2 μg/ml) were mixed and incubated in the dark for 12 h. The ultraviolet absorption at 425 nm was detected to measure the clearance rate of H_2O_2.

The $ONOO^-$ scavenging ability of TWNDs was evaluated by UV–Vis spectroscopy using pyrogallol red as the indicator. Briefly, pyrogallol red (5 mM), $ONOO^-$ and TWNDs with different concentration (0 mM, 0.3 mM, 0.6 mM, 1 mM, 2 mM, 4 mM, 6 mM, 8 mM) were mixed and reacted for 15 min. Afterward, the ultraviolet absorption spectrum was scanned to measure the clearance rate of $ONOO^-$.

4.8. XPS measurement of TWNDs

X-ray photoelectron spectroscopy (XPS) was conducted for the element/chemical state analysis of TWNDs. Firstly, we scanned the full spectrum of tannic acid, phosphotungstic acid, and TWNDs. Afterward, the XPS measurement of TWNDs was performed before and after incubation with various ROS ($O_2^{-\cdot}$, $OH^{-\cdot}$, H_2O_2, and $ONOO^-$).

4.9. Hemolysis-induced and CP-AKI models

Institute of Cancer Research (ICR) mice (female, 4–6 weeks old, 20–25 g) and C57 BL/6 mice (male, 4–6 weeks old, 20–25 g) were purchased from Hunan STA Laboratory Animal CO., LTD (Changsha, China). All animal experiments use protocol has been approved by the Institutional Animal Care and Use Committee (IACUC), Xiangya Hospital, Central South University, China. For hemolysis-induced AKI models, all ICR mice were given food but no water for 15 h. At the end of water restriction, 50% glycerol (8 mL/kg) was then intramuscularly injected into both hind limbs, and all mice were then given free access to water and food. For CP-AKI models, all C57BL/6 mice were received intraperitoneal injections of CP (20 mg/kg). At 2 h after glycerol or CP injection, mice were used as AKI model for further study.

4.10. Treatment of AKI mice

Two hours after the AKI model induction, different treatments were performed on hemolysis-induced AKI model mice: group 1 was healthy mice treated with 1 × PBS; group 2 was healthy mice treated with TWNDs (32 mg/kg in 100 μl PBS), group 3 was AKI mice treated with 1 × PBS; group 4, 5, 6 were AKI mice treated with TWNDs (4, 8 and 16 mg/kg in 100 μl PBS, respectively); group 7 was positive control group that AKI mice treated with NAC (130 mg/kg in 100 μl PBS); group 8, 9, 10 were negative control group that AKI mice treated with phosphotungstic acid (WU), tannic acid (TA) and NAC (4 mg/kg in 100 μl PBS, respectively) (n = 6 in each group). Heathy C57/BL6 and CP-AKI mice were divided into 4 groups: group 1 was healthy mice treated with 1 × PBS; group 2 was CP-AKI mice treated with 1 × PBS; group 3 were CP-

AKI mice treated with TWNDs (4 mg/kg in 100 μl PBS); group 4 was CP-AKI mice treated with NAC (130 mg/kg in 100 μl PBS) (n = 6 in each group). All treated reagents were injected through tail vein.

4.11. Evaluation of treatment effects on AKI status

The therapeutic efficacy of TWNDs in AKI models was evaluated by kidney function tests and H&E staining. The glycerol induced AKI mice were euthanized after 24 h treated. The CP-AKI mice were euthanized after 72 h treated. The body weight of AKI mice was monitored. The blood was collected and serum was isolated through centrifugations at 2000 g/min for 15 min. BUN and creatinine levels in the plasma were analyzed using automatic biochemistry analyzer BS-2000 M (Mindray, Shenzhen, China). For H&E staining analysis, the collected renal tissues were fixed with 4% paraformaldehyde and embedded in paraffin, followed by sectioning and H&E staining.

4.12. Assessment of renal superoxide production

After treatment, the kidneys of mice were collected and stored in optimum cutting temperature (O.C.T.) specimen matrix for cryostat sectioning at −20 °C. The frozen kidneys were further sectioned into tissue slices (approximately 5 μm thickness) using the Cryotome E freezing microtome (Thermo Carlsbad,CA, USA). To assess superoxide production histologically, frozen kidney tissue slices were washed with 1 × PBS and stained with DHE (10 μM) for 30 min. Then incubate with DAPI solution at RT for 10 min. After wash three times with PBS, a cover glass was further used to each slide with anti-fade mounting medium (Servicebio, Wuhan, China). And fluorescent imaging was recorded on Ortho-Fluorescent Microscopy (Nikon ECLIPSE C1).

4.13. Transmission electron microscopy (TEM) of kidney

The targeted tissue was fixed in fresh TEM fixation. And then wash the tissues using 0.1 M PBS (pH 7.4) for 3 times, 15 min each. Tissues avoid light post fixed with 1% OsO_4 in 0.1 M PB (pH 7.4) for 2 h at RT. After remove OsO4, the tissues are rinsed in 0.1 M PB (pH 7.4) for 3 times, 15 min each. After dehydrate at RT, the tissue was Resin penetration and embedding, polymerization. The resin blocks were cut to 60–80 nm thin on the ultramicrotome, and the tissues were fished out onto the 150 meshes cuprum grids with formvar film. 2% uranium acetate saturated alcohol solution avoid light staining for 8 min, rinsed in 70% ethanol for 3 times and then rinsed in ultrapure water for 3 times. 2.6% Lead citrate avoid CO_2 staining for 8 min, and then rinsed with ultrapure water for 3 times. After dried by the filer paper, the cuprum grids were put into the grids board and dried overnight at RT. The cuprum grids are observed under TEM (HITACHI HT7800/HT77000) and take images.

4.14. In vivo toxicity assessment

Healthy ICR mice were randomized into two groups. The control group, consisted of healthy mice injected with 100 μl of 1 × PBS (n = 6); the TWNDs group consisted of healthy mice injected with 100 μl of TWNDs 32 mg/kg in 1 × PBS (n = 6). The mice were euthanized at 24 h post-injection. Subsequently, the major organs (heart, liver, spleen, lung, and kidney) and blood were harvested. Histological changes in organs were analyzed by H&E staining, and whole blood samples were used for hematology analysis (Sysmex XE-2100, Kobe, Japan). The analyzed blood parameters were as follows: white blood cells (WBC), lymphocytes (LYM), monocytes (MON), red blood cells (RBC), hemoglobin (HGB), mean corpuscular hemoglobin (MCH), the hematocrit (HCT), corpuscular volume (MCV), mean corpuscular hemoglobin concentration (MCHC), mean platelets (PLT), platelet distribution width (PDW), mean platelet volume (MPV), red cell distribution width (RDW) and the plateletcrit (PCT). Indicators of hepatic function (alanine aminotransferase (ALT) and aspartate aminotransferase (AST)) and kidney function (BUN and creatinine levels) were analysis using automatic biochemistry analyzer BS-2000 M. For long toxicity test, the healthy mice were injected with 100 μl of TWNDs 32 mg/kg in 1 × PBS for 30 days (n = 6).

4.15. Cells culture

HK-2 cells were cultured in DMEM/nutrient mixture F-12 (DMEM/F12) with 10% fetal bovine serum. RAW 264.7 macrophage cells were cultured in DMEM with 10% newborn calf serum. All cells were purchased from National Collection of Authenticated Cell Cultures of China and maintained at 37 °C in 5% CO_2 and a humidified atmosphere.

4.16. Free radical scavenging with TWNDs in cells

The HK-2 cells were seeded into a 96-well plate at 1×10^4/well, then incubated for 24 h. The TWNDs were dispersed in culture media at different concentrations (5, 10, 25, 50, and 100 μg/mL, respectively) followed with H_2O_2 (500 μM). After 4 h incubation under 5% CO_2 at 37 °C, cell viability was determined by CCK-8 assay and cell apoptosis. To reliably measure levels of ROS in live cells, 10 μM of a DCFH-DA ROS probe (CA1410, Solarbio, Beijng, China) was added to each well after TWNDs incubation and H_2O_2 treatment. Then, the cells were washed with 1 × PBS three times, and measured for emission at 525 nm with an excitation of 488 nm.

4.17. Mitochondrial function

Living HK-2 cells after different treated were labeled with 5 μM MitoSOX™ reagent for 10 min at 37 °C followed with Hoechst 33342 Staining Solution for Live Cells and mount in warm buffer. Mitochondrial membrane potential was measured using JC-1 staining working solution at 37 °C for 15 min. After incubation, the cells were washed for several times and examined using flow cytometry or fluorescence microscope.

4.18. ATP assays

HK-2 cells with different treated were collected by centrifugation (14,000 g, 4 °C, 2min) and washed with prechilled PBS. The cells were then lysed using the lysis buffer in the Enhanced ATP Assay Kit. The ATP content was determined according to the manufacturer's instructions. Detecting solution was added to a white 96-well plate and incubated at RT for 5min. Then the supernatant collected from lysed cells was mixed with detecting solution quickly, and read in 30 min. Total ATP concentrations were calculated according to the luminescence signals and were normalized by the protein levels.

4.19. Immunofluorescence staining

RAW 264.7 cells grown on coverslips washed with PBS twice and fixed with 4% paraformaldehyde. After washed with PBS for 5 times, the cells were permeabilized by incubation in 0.1% Triton X-100 in PBS for 5 min on ice, followed by washing with PBS twice. The cells were then blocked with blocking buffer (2% BSA in PBS) at RT for 1 h. Then exposed to a primary rabbit anti-COX-2 antibody. After a 2 h incubation in 37 °C, cells were washed with PBS, then exposed to Alexa Fluor-594-conjugated goat-anti-rabbit. Then exposed to the second primary rabbit tubulin beta antibody. After a 2 h incubation in 37 °C, cells were washed with PBS, then exposed to Alexa Fluor-488-conjugated goat-anti-rabbit. After 30 min of incubation, cells were washed free of secondary antibody with PBS. Nuclei were counterstained with ProLong™ Glass Antifade Mountant with NucBlue™ Stain. Cells were then imaged using a Leica Confocal laser scanning microscope (CLSM) SP8 inverted confocal microscope with a 63 × oil objective. Fluorescence probes were excited by

three separate laser lines (552, 405, and 488 nm) and monitored at the respective emission wavelength ranges under the control of Leica software (Leica).

4.20. Immunohistochemical (IHC) analysis

The left kidney tissue was fixed in 4% paraformaldehyde and embedded in paraffin. The paraffin sections (5 μm) were mounted onto slides and deparaffinized with xylene for 7 min (three times). The slides were rehydrated gradually in a graded series of alcohol and washed with deionized water. They were washed with PBS and then treated with 3% H_2O_2 in methanol for 20 min at RT to quench endogenous peroxide activity. To expose antigens, kidney sections were boiled in a target retrieval solution (0.01 M sodium citrate, pH 6.0) for 10 min. The slides were then incubated overnight with the Cyt *c* antibody and F4/80 antibody at 4 °C and then washed with PBS. Protein expression in tissue sections was detected using the Histostain-Plus Kits, according to the manufacturer's protocol. The sections were observed under a light microscope.

4.21. Apoptosis analysis

For Annexin V FITC (CA1020, Solarbio), HK-2 cells were collected by trypsinization, washed twice in cold FBS, pelleted by centrifugation and resuspended with 1 × binding buffer to a final concentration of 1×10^6 cells/ml. 5 μl of Annexin V FITC and propidium iodide were added to 100 μl of single cell suspension and incubated for 15min at RT in the dark. After 1 × binding buffer was added, cells were analyzed by a novocyte3130 flow cytometry (Agilent). Kidney tissue apoptosis was measure using TUNEL staining according to the manufacture's protocol, and staining was observed under fluorescence microscope.

4.22. Statistical analysis

Quantitative data were presented as mean ± standard deviation (S.D.). One-way analysis of variance was performed to determine the statistical differences. Differences were accepted as significant at a *P*-value lower than 0.05. SPSS 21.0 software was used for statistical analyses (SPSS Inc., USA).

CRediT authorship contribution statement

Qiong Huang: Conceptualization, Methodology, Project administration, Writing – original draft. **Yuqi Yang:** Investigation, Formal analysis, Visualization. **Tianjiao Zhao:** Resources, Investigation, Data curation. **Qiaohui Chen:** Data curation, Visualization. **Min Liu:** Formal analysis. **Shuting Ji:** Writing – review & editing. **Yan Zhu:** Data curation, Investigation. **Yunrong Yang:** Data curation, Investigation. **Jinping Zhang:** Investigation. **Haixin Zhao:** Validation, Resources. **Yayun Nan:** Writing – review & editing. **Kelong Ai:** Conceptualization, Writing – review & editing, Supervision, Project administration.

Declaration of competing interest

The authors declare no conflict of interest, financial or otherwise.

Acknowledgement

This work was supported by the National Natural Science Foundation of China (No. 81974508, 21974134), the Hunan Science Fund for Distinguished Young Scholar of China (No. 2021JJ10067), Innovation-Driven Project of Central South University (No. 202045005), Hunan Provincial Natural Science Foundation of China (No. 2021JJ31066), Key Research Project of Ningxia Hui Autonomous Region in 2021 of China (Major Project) (No. 2021BEG01001), Key Program of Ningxia Hui Autonomous Region Natural Science Foundation of China (No. 2022JJ21059).

Appendix A. Supplementary data

Supplementary data to this article can be found online at https://doi.org/10.1016/j.bioactmat.2022.08.022.

References

[1] J.A. Kellum, P. Romagnani, G. Ashuntantang, C. Ronco, A. Zarbock, H.-J. Anders, Nat. Rev. Dis. Prim. 7 (2021) 52.
[2] D.A.C. Messerer, R. Halbgebauer, B. Nilsson, H. Pavenstädt, P. Radermacher, M. Huber-Lang, Nat. Rev. Nephrol. 17 (2021) 91.
[3] C. Ronco, R. Bellomo, J.A. Kellum, Lancet (London, England) 394 (2019) 1949.
[4] M.K. Nadim, L.C. Forni, R.L. Mehta, M.J. Connor, K.D. Liu, M. Ostermann, T. Rimmele, A. Zarbock, S. Bell, A. Bihorac, V. Cantaluppi, E. Hoste, F. Husain-Syed, M.J. Germain, S.L. Goldstein, S. Gupta, M. Joannidis, K. Kashani, J.L. Koyner, M. Legrand, N. Lumlertgul, S. Mohan, N. Pannu, Z.Y. Peng, X.L. Perez-Fernandez, P. Pickkers, J. Prowle, T. Reis, N. Srisawat, A. Tolwani, A. Vijayan, G. Villa, L. Yang, C. Ronco, J.A. Kellum, Nat. Rev. Nephrol. 16 (2020) 747.
[5] S. Sawhney, A. Marks, N. Fluck, A. Levin, G. Prescott, C. Black, Am. J. Kidney Dis. : the official journal of the National Kidney Foundation 69 (2017) 18.
[6] C. Tang, J. Cai, X.M. Yin, J.M. Weinberg, M.A. Venkatachalam, Z. Dong, Nat. Rev. Nephrol. 17 (2021) 299.
[7] S.R. Gonsalez, A.L. Cortês, R.C.D. Silva, J. Lowe, M.C. Prieto, L.D. Silva Lara, Pharmacol. Therapeut. 200 (2019) 1.
[8] M. Ostermann, A. Zarbock, S. Goldstein, K. Kashani, E. Macedo, R. Murugan, M. Bell, L. Forni, L. Guzzi, M. Joannidis, S.L. Kane-Gill, M. Legrand, R. Mehta, P. T. Murray, P. Pickkers, M. Plebani, J. Prowle, Z. Ricci, T. Rimmelé, M. Rosner, A. D. Shaw, J.A. Kellum, C. Ronco, JAMA Netw. Open 3 (2020), e2019209.
[9] S.Y. Robbins-Juarez, L. Qian, K.L. King, J.S. Stevens, S.A. Husain, J. Radhakrishnan, S. Mohan, Kidney international reports 5 (2020) 1149.
[10] J.S. Hirsch, J.H. Ng, D.W. Ross, P. Sharma, H.H. Shah, R.L. Barnett, A.D. Hazzan, S. Fishbane, K.D. Jhaveri, C.-R.C. Northwell, C.-R.C. Northwell Nephrology, Kidney Int. 98 (2020) 209.
[11] Z. Zhou, K. Ni, H. Deng, X. Chen, Adv. Drug Deliv. Rev. 158 (2020) 73;
[a] H. Wang, D. Yu, J. Fang, Y. Zhou, D. Li, Z. Liu, J. Ren, X. Qu, Chem. Sci. 11 (2020), 12721.
[12] L. Wang, Y. Zhang, Y. Li, J. Chen, W. Lin, Nano Res. 14 (2021) 920.
[13] J. Dan Dunn, L.A.J. Alvarez, X. Zhang, T. Soldati, Redox Biol. 6 (2015) 472.
[14] H.Q. Lai, X.B. Zhang, Z.H. Song, Z.W. Yuan, L.Z. He, T.F. Chen, Chem. Eng. J. 391 (2020) 11;
[a] S.H. Jung, W. Lee, S.H. Park, K.Y. Lee, Y.J. Choi, S. Choi, D. Kang, S. Kim, T. S. Chang, S.S. Hong, B.H. Lee, Redox Biol. 37 (2020), 101751;
[b] Cao, L. Zhang, Y. You, L. Zheng, J. Ren, X. Qu, Angew. Chem. Int. Ed. 59 (2020) 5108.
[15] L. Jiang, S. Zhou, X. Zhang, C. Li, S. Ji, H. Mao, X. Jiang, Nat. Commun. 12 (2021) 2390;
[a] F. Xu, X. Huang, Y. Wang, S. Zhou, Adv. Mater. 32 (2020), 1906745;
[b] Y. Zhang, A. Khalique, X. Du, Z. Gao, J. Wu, X. Zhang, R. Zhang, Z. Sun, Q. Liu, Z. Xu, A.C. Midgley, L. Wang, X. Yan, J. Zhuang, D. Kong, X. Huang, Adv. Mater. 33 (2021), 2006570.
[16] J. Shen, T.W. Rees, Z. Zhou, S. Yang, L. Ji, H. Chao, Biomaterials 251 (2020), 120079.
[17] G. Battogtokh, Y.S. Choi, D.S. Kang, S.J. Park, M.S. Shim, K.M. Huh, Y.Y. Cho, J. Y. Lee, H.S. Lee, H.C. Kang, Acta Pharm. Sin. B 8 (2018) 862.
[18] D. Liu, G. Shu, F. Jin, J. Qi, X. Xu, Y. Du, H. Yu, J. Wang, M. Sun, Y. You, M. Zhu, M. Chen, L. Zhu, Q. Shen, X. Ying, X. Lou, S. Jiang, Y. Du, Sci. Adv. 6 (2020), eabb7422.
[19] Z. Li, X. Shan, Z. Chen, N. Gao, W. Zeng, X. Zeng, L. Mei, Adv. Sci. 8 (2021), 2002589.
[20] D. Liu, F.Y. Jin, G.F. Shu, X.L. Xu, J. Qi, X.Q. Kang, H. Yu, K.J. Lu, S.P. Jiang, F. Han, J. You, Y.Z. Du, J.O. Ji, Biomaterials 211 (2019) 57;
[a] H. Yu, F.Y. Jin, D. Liu, G.F. Shu, X.J. Wang, J. Qi, M.C. Sun, P. Yang, S. P. Jiang, X.Y. Ying, Y.Z. Du, Theranostics 10 (2020) 2342.
[21] B.C. Liu, T.T. Tang, L.L. Lv, H.Y. Lan, Kidney Int. 93 (2018) 568.
[22] Y. Ma, F. Cai, Y. Li, J. Chen, F. Han, W. Lin, Bioact. Mater. 5 (2020) 732.
[23] D.L. Ni, D.W. Jiang, C.J. Kutyreff, J.H. Lai, Y.J. Yan, T.E. Barnhart, B. Yu, H.J. Im, L. Kang, S.Y. Cho, Z.F. Liu, P. Huang, J.W. Engle, W.B. Cai, Nat. Commun. 9 (2018) 11;
[a] A.S. Cherevan, S.P. Nandan, I. Roger, R. Liu, C. Streb, D. Eder, Adv. Sci. 7 (2020), 1903511.
[24] M. Zhou, Y. Liu, Y. Su, Q. Su, Advanced Healthcare Materials 10 (2021), 2101331;
[a] J.P. Sheng, L. Zhang, L. Deng, Y.J. Han, L.Q. Wang, H.C. He, Y.N. Liu, Chem. Eng. J. 383 (2020), 123071.
[25] C. He, S. Qiu, S. Sun, Q. Zhang, G. Lin, S. Lei, X. Han, Y. Yang, ENERGY & ENVIRONMENTAL MATERIALS 1 (2018) 88.
[26] P. Bhargava, R.G. Schnellmann, Nat. Rev. Nephrol. 13 (2017) 629.
[27] J. Qiu, Q. Xiao, X. Zheng, L. Zhang, H. Xing, D. Ni, Y. Liu, S. Zhang, Q. Ren, Y. Hua, K. Zhao, W. Bu, Nano Res. 8 (2015) 3580;
[a] Z. Xiao, C. Peng, X. Jiang, Y. Peng, X. Huang, G. Guan, W. Zhang, X. Liu, Z. Qin, J. Hu, Nanoscale 8 (2016), 12917.

[28] D.Y. Zhang, H.K. Liu, M.R. Younis, S. Lei, C. Yang, J. Lin, J.L. Qu, P. Huang, Chem. Eng. J. 409 (2021) 13.
[29] K. Ai, Y. Liu, L. Lu, J. Am. Chem. Soc. 131 (2009) 9496.
[30] J. Wang, L. Sui, J. Huang, L. Miao, Y. Nie, K. Wang, Z. Yang, Q. Huang, X. Gong, Y. Nan, K. Ai, Bioact. Mater. 6 (2021) 4209.
[31] X. Zhao, L.-Y. Wang, J.-M. Li, L.-M. Peng, C.-Y. Tang, X.-J. Zha, K. Ke, M.-B. Yang, B.-H. Su, W. Yang, Adv. Sci. (2021), 2101498.
[32] J.J. Hou, H. Wang, Z.L. Ge, T.T. Zuo, Q. Chen, X.G. Liu, S. Mou, C.H. Fan, Y. Xie, L. H. Wang, Nano Lett. 20 (2020) 1447.
[33] K.M. Ralto, E.P. Rhee, S.M. Parikh, Nat. Rev. Nephrol. 16 (2020) 99.
[34] P. Bhargava, R.G. Schnellmann, Nat. Rev. Nephrol. 13 (2017) 629.
[35] C. Garrido, L. Galluzzi, M. Brunet, P.E. Puig, C. Didelot, G. Kroemer, Cell Death Differ. 13 (2006) 1423.
[36] K. McArthur, L.W. Whitehead, J.M. Heddleston, L. Li, B.S. Padman, V. Oorschot, N. D. Geoghegan, S. Chappaz, S. Davidson, H. San Chin, R.M. Lane, M. Dramicanin, T. L. Saunders, C. Sugiana, R. Lessene, L.D. Osellame, T.L. Chew, G. Dewson, M. Lazarou, G. Ramm, G. Lessene, M.T. Ryan, K.L. Rogers, M.F. van Delft, B.T. Kile, Science (New York, N.Y.) 359 (2018), eaao6047.
[37] F.J. Bock, S.W.G. Tait, Nat. Rev. Mol. Cell Biol. 21 (2020) 85.
[38] Å.B. Gustafsson, G.W. Dorn, Physiol. Rev. 99 (2019) 853.
[39] V. Cohen-Kaplan, I. Livneh, N. Avni, B. Fabre, T. Ziv, T. Kwon Yong, A. Ciechanover, Proc. Natl. Acad. Sci. USA 113 (2016) E7490.
[40] S. Kageyama, S.R. Gudmundsson, Y.-S. Sou, Y. Ichimura, N. Tamura, S. Kazuno, T. Ueno, Y. Miura, D. Noshiro, M. Abe, T. Mizushima, N. Miura, S. Okuda, H. Motohashi, J.-A. Lee, K. Sakimura, T. Ohe, N.N. Noda, S. Waguri, E.-L. Eskelinen, M. Komatsu, Nat. Commun. 12 (2021) 16.
[41] D. Vijayan, A. Young, M.W.L. Teng, M.J. Smyth, Nat. Rev. Cancer 17 (2017) 709; [a] J. Fucikova, R. Spisek, G. Kroemer, L. Galluzzi, Cell Res. 31 (2021) 5.
[42] M. Mittal, M.R. Siddiqui, K. Tran, S.P. Reddy, A.B. Malik, Antioxidants Redox Signal. 20 (2013) 1126; [a] L. Chen, Q. Huang, T. Zhao, L. Sui, S. Wang, Z. Xiao, Y. Nan, K. Ai, Redox Biol. 45 (2021), 102046; [b] T. Zhao, W. Wu, L. Sui, Q. Huang, Y. Nan, J. Liu, K. Ai, Bioact. Mater. 7 (2022) 47.
[43] M.N. Jeffres, Drugs 77 (2017) 1143.
[44] Q. Chen, F. Ding, S. Zhang, Q. Li, X. Liu, H. Song, X. Zuo, C. Fan, S. Mou, Z. Ge, Nano Lett. 21 (2021) 4394; [a] D.Y. Zhang, M.R. Younis, H.K. Liu, S. Lei, Y.L. Wan, J.L. Qu, J. Lin, P. Huang, Biomaterials 271 (2021) 12.
[45] J.Y.C. Soo, J. Jansen, R. Masereeuw, M.H. Little, Nat. Rev. Nephrol. 14 (2018) 378.